Signatures of Synchrotron Radiation from the Relativistic Jet Base

Oliver Porth[1], Christian Fendt[1], Zakaria Meliani[2] & Bhargav Vaidya[1]

[1]Max Planck Institut für Astronomie, Heidelberg - Germany

[2]Centre for Plasma Astrophysics, K.U. Leuven - Belgium

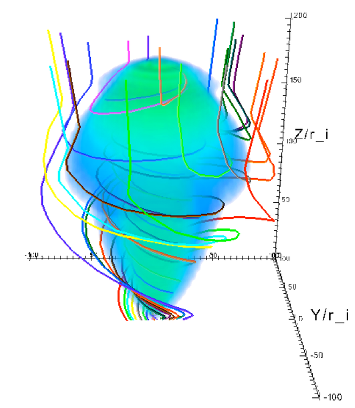

Abstract

Synchrotron radiation from relativistic jets is a frequent accompaniment of Active Galactic Nuclei. In the current paradigm of relativistic magnetohydrodynamic (MHD) jet formation, the jets are accelerated and collimated over distances possibly extending out to parsec scale. However large in terms of the launching environment, this inner region of the AGN jet can barely be resolved and is therefore often imaged as a compact, optically thick radio core.

The goal of the present work is to derive observational signatures from state-of-the-art simulation models of collimating MHD jets featuring a large-scale helical magnetic field on the parsec scale to facilitate the interpretation of AGN jet observations.

We perform axisymmetric special relativistic magnetohydrodynamic simulations of the jet formation region using the PLUTO 3.01 code. Applying the resulting magnetohydrodynamic jet structure we solve the linearly polarized synchrotron radiation transport taking into account self-absorption and internal Faraday rotation to produce realistic synchrotron maps in the radio and mm wavelengths.

From the Stokes parameters, we derive VLBI radio and (sub-) mm diagnostics such as core shift, polarization structure, intensity maps, spectra and Faraday rotation measure (RM). We investigate depolarization and the detectability of a λ^2-law RM with corresponding gradients depending on beam resolution and observing frequency.

Simulation setup

The simulations are performed on an axisymmetric grid in cylindrical coordinates.
Main characteristics are:

- Injection boundary modeling accretion disk corona
- Causal equation of state
- Hot inner plasma $c_p/c_v \simeq 4/3$ accelerated thermally [1] $\Gamma \to 3$
- Hadronic Poynting dominated disk wind [2], $c_p/c_v \simeq 5/3, \Gamma \to 8$
- PLUTO 3.01 RMHD code, hll Rieman solver
- Grid: Stretched 2555^2 cells in (r,z) plane covering 2000^2 inner disk radii
- Free outflow boundaries out of causal contact with solution
- Pointmass (Newtonian-) gravity for stratification
- Injection with slow-magnetosonic velocity

The disk-boundary represents the corona of an accretion disk driving a global current system. We prescribe various current distributions via the boundary toroidal magnetic field investigating open current circuits as well as currents that are closed within the jet. Profiles for $\{\rho, p, B_\phi, v_p, E_\phi\}$ are assigned as fixed in time boundary conditions.

Overview of simulations

Governing parameters of the MHD simulations are the disk toroidal field power-law index s, where $B_\phi \propto r^{-s}$ and the (poloidal) plasma-β at the inner disk radius β_1. The simulations are performed on the JADE cluster in Montpellier featuring 512 cores with a typical run-time of 20K cpu hours. The table gives an overview of the simulations.

run ID	s	β_1	$\Gamma_{\rm max}$	Γ_∞	$\theta_{\rm fl,1}$
1h	1	0.005	8.5	25	0.21°
2h	1.25	0.005	7.9	24	0.16°
3h	1.5	0.005	7.9	23	0.17°
1m	1	0.01	5.9	13	0.14°
2m	1.25	0.01	5.6	13	0.16°
3m	1.5	0.01	5.9	13	0.24°

Columns denote: Simulation ID; Radial power law slope of the toroidal field; Plasma beta at (r,z)=(1,0); Maximal Lorentz factor obtained in the Raycasting domain; Maximal conserved energy flux; Collimation angle of the field line rooted at the inner disk radius evaluated at z=1000.

Jet acceleration

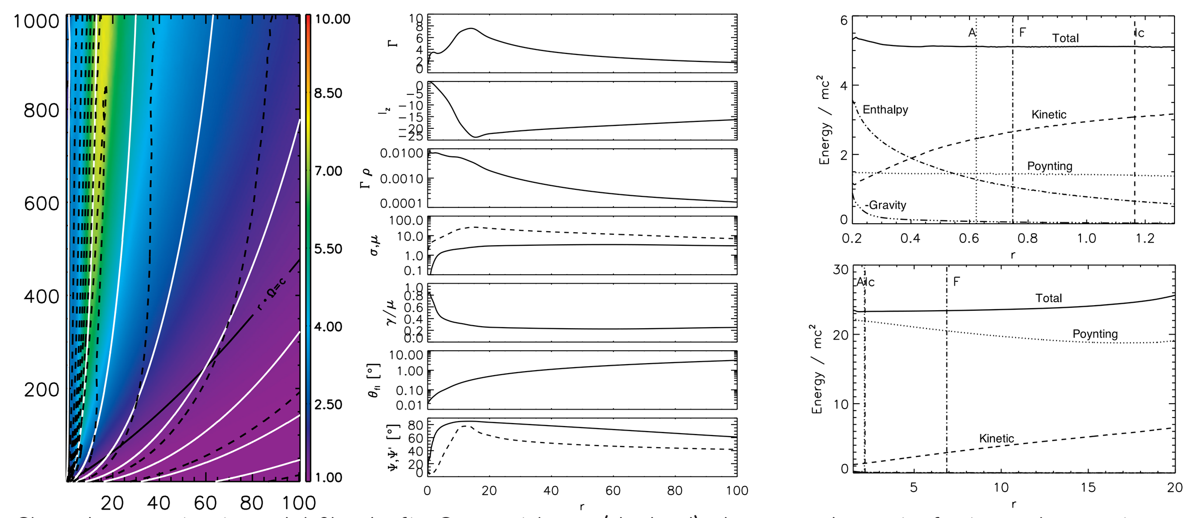

Closed current jet model 2h. *Left:* Current lines (dashed) shown on Lorentz factor color-contours in the (r,z) plane. *Center:* Cuts through $z = 750$ for Lorentz-factor Γ, integral current I_z and various other quantities. *Right:* Acceleration along selected field-lines against the cylindrical radius r showing thermal acceleration for a field line in the spine (footpoint $r_{\rm fp} = 0.2$, above) and magnetic acceleration in the jet ($r_{\rm fp} = 1.5$, below). Vertical lines indicate the crossing of the Alfvèn (A) and fast (F) critical point as well as the light cylinder (lc).

Stokes vector transport

For a grid of lines of sight, we solve the linearly polarized radiation transport $\frac{d\mathbf{I}}{dl} = \boldsymbol{\mathcal{E}} - \underline{\mathbf{A}}\,\mathbf{I}$ for the Stokes parameters $\mathbf{I} = \{I^l, I^r, U\}$

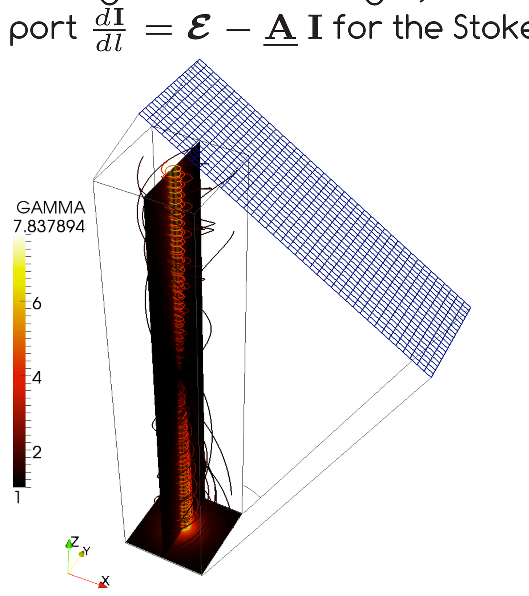

where $\boldsymbol{\mathcal{E}}$ denotes the emissivity vector and $\underline{A}$ the opacity matrix, taking into account

- Beaming and aberration
- Swing of the polarization direction
- Internal Faraday rotation

of the relativistically moving plasma allowing a detailed study of intensity, depolarization, polarization and Faraday rotation structure.

Raytracing for an exemplary line of sight. Thick blue lines including Faraday rotation compared to a case where the latter was neglected. The upper panels show intensity, the Stokes parameters and U (second panel). Faraday opacity, polarization degree and the optical depth is shown in the subsequent panels. Internal Faraday rotation and the accompanying depolarization is observed in the emitting region near the $x = 0$ plane ($l = 0$).

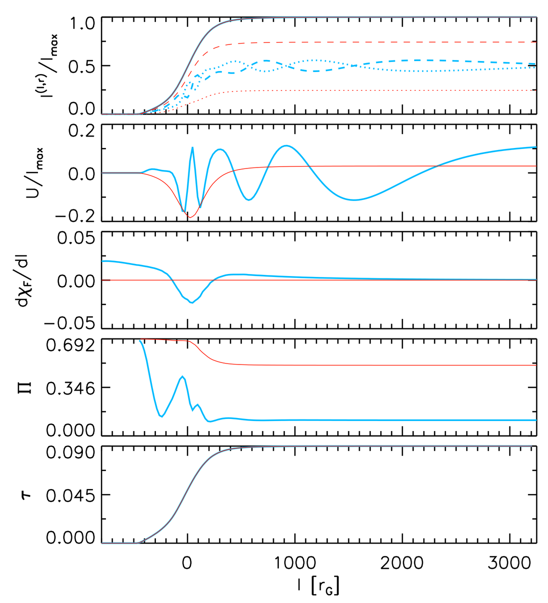

Particle acceleration

A radiation model comprises a MHD simulation run, a particular physical scaling given by black hole mass $M_\bullet$ and jet energy flux $\dot{E}$ and the specific parameters of the radiation transport. A distribution for the relativistic electrons of $dn_{\rm e} = N_0 E^{-0.5} dE$ is assumed. Here we model the emitting region via its minimal co-moving pitch angle Ψ' and assume quasi-equipartition between relativistic particles and magnetic field strength with equipartition fraction $\epsilon_{\rm B}$. We have also compared various tracers for the relativistic electrons [3].

model ID	run ID	$M_\bullet[M_\odot]$	$\dot{E}[{\rm erg/s}]$	$\epsilon_{\rm B}$	$\tan\Psi'$	$\frac{\dot{M}}{\dot{M}_{\rm Edd}}$
A	2h	10^9	10^{43}	0.1	1	1.3×10^{-6}
B	2h	10^9	10^{44}	0.001	0.5	1.3×10^{-5}

Jet radiation

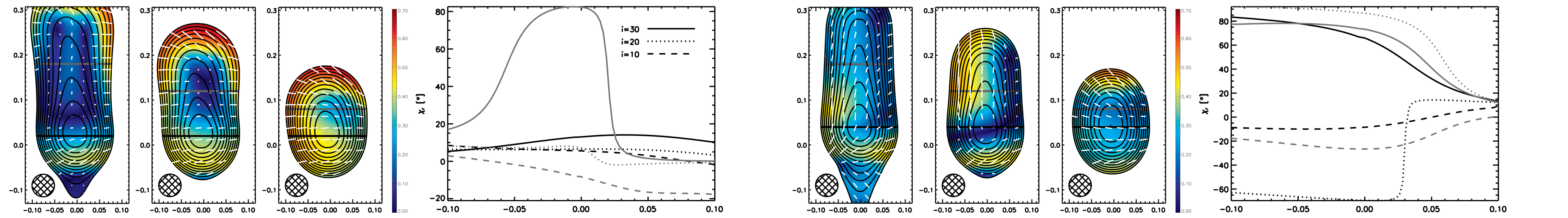

Polarizations for $i \in \{30^\circ, 20^\circ, 10^\circ\}$ *(from left to right)* emitted from regions with co-moving pinches $B'_\phi/B'_p > 1$ *(left panels)* and $B'_\phi/B'_p > 2$ *(right panels)* neglecting Faraday rotation. The polarization degree $\Pi_{43\rm GHz}$ is color-coded and $I_{43\rm GHz}$ contours are shown. Contours are spaced by a factor of 2 out to $\simeq 5 \cdot 10^{-4} I_{\nu,\rm peak}$ where the image is cropped. Spatial scale is given in milli arcseconds and a restoring beam with FWHM=$0.05\,\rm mas$ was used. The right-hand panel shows polarization angles along the cuts along core *(black)* and jet *(gray)*.

Faraday rotation measure

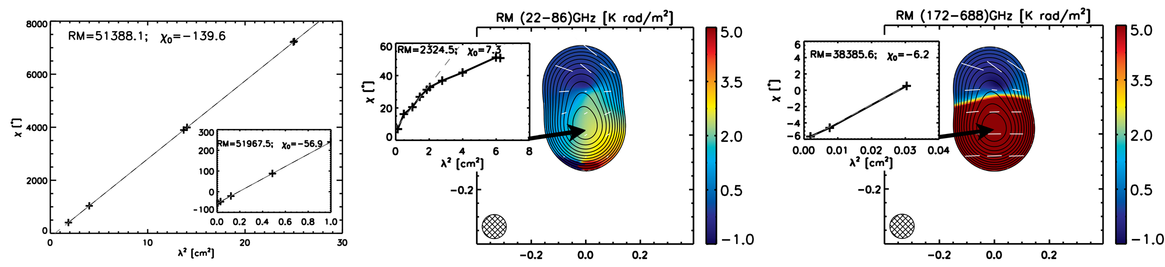

Determination of the rotation measure $\chi(\lambda^2) = \chi_0 + {\rm RM}\lambda^2$ in model A. *Left:* Fit for an ideal resolution line of sight. *Right:* Reconstruction of the RM after beam convolution in the optically thick (22-86 GHz) and optically thin (172-688 GHz) regime. The effective emission angle χ_0 is indicated by white sticks.

Consistent λ^2-law rotation measures can be reproduced in ideal resolution in both regimes. Once beam convolution is taken into account, unresolved core shifts can break the λ^2-law in the optically thick case.

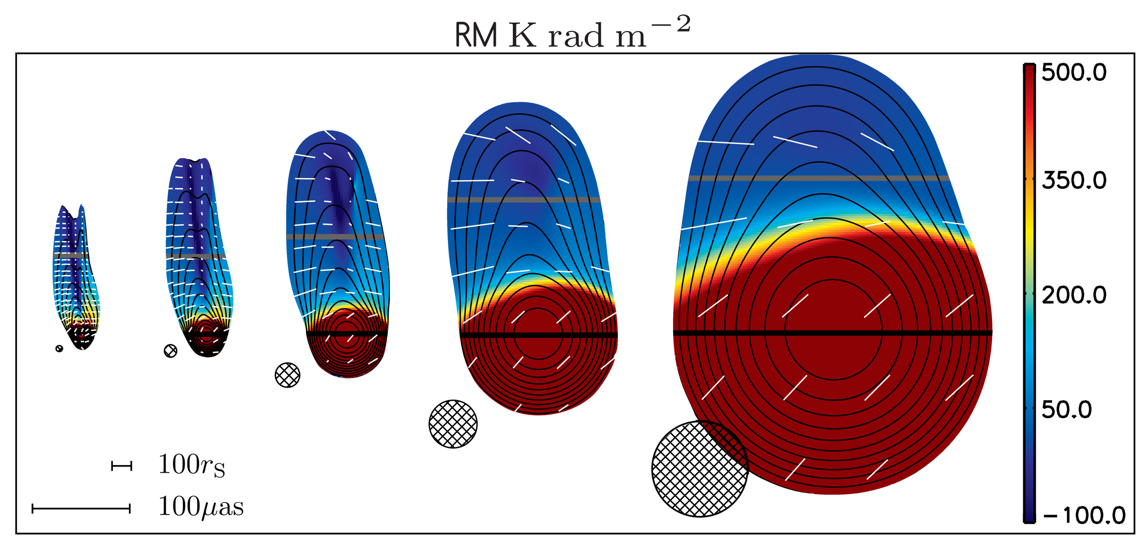

Effect of resolution on the detectability of transversal rotation measure gradients, model B.

Top: RM maps in the optically thin wavelength range when observed with decreasing resolution from 6.25μas to 100μas. *Right:* Cuts along the indicated paths. 3° detection limits for $86 - 688\,\rm GHz$ and $172 - 688\,\rm GHz$ observations are shaded grey.

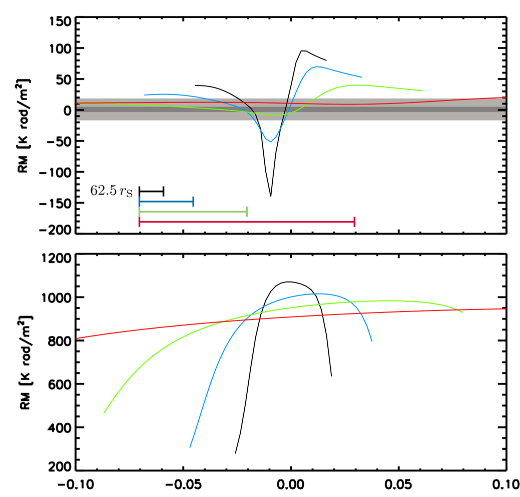

Viewing angle

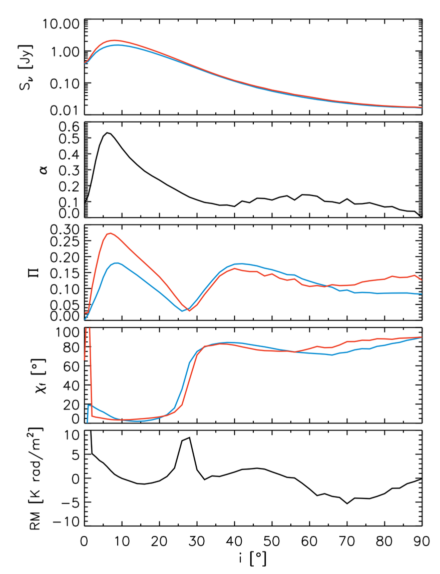

Unresolved quantities in dependence of the viewing angle i for 86 GHz (red) and 43 GHz (blue) for model A.

The dominating polarization direction flips from perpendicular (0°) to parallel (90°) for viewing angles $i > 25^\circ$. At this flip, the polarization degree shows a local minimum through beam depolarization. For $i = 0^\circ$, the polarization degree approaches zero and its direction fluctuates between 0° and 90° due to the axial symmetry.

Conclusions

- The Poynting dominated disk wind develops into a jet with Lorentz factors of $\Gamma \simeq 8$ within the computational domain and is collimated to $< 1^\circ$ in the linear acceleration regime $\Gamma \propto r$. We do not recover the tight correlation $\Gamma\theta_{\rm fl} \simeq 1$ between acceleration and collimation suggested for ultra-relativistic jets.
- Asymmetric half spine-sheath polarization structures allow the measurement of the handedness of the helical magnetic field and thus indirectly the spin direction of the central engine.
- The intrinsic RM profiles across the jet are non-monotonic. A resolution of $\sim 100 r_{\rm S}$ would be required for their detection.
- In our realistic - collimating - jet geometry, the strict bi-modality in polarization direction as it was predicted for optically thin axial jets by Pariev et al. can be circumvented. For the radiation originating in the high-speed collimated asymptotic jet flow however, we recover the bi-modal alignment.
- If the polarization signal is not scrambled by high Faraday rotation, our model (A) implies that the unresolved optically thin electric polarization vector in blazar sources are aligned perpendicular to the projected jet direction, while for higher inclination the polarization flips to a parallel alignment.

Future high frequency sub-mm surveys will be able to test these conjectures.

References

[1] Z. Meliani, C. Sauty, K. Tsinganos, E. Trussoni, and V. Cayatte. Relativistic spine jets from Schwarzschild black holes. Application to AGN radio-loud sources. *A&A*, 521:A67+, Oct. 2010.

[2] O. Porth and C. Fendt. Acceleration and Collimation of Relativistic Magnetohydrodynamic Disk Winds. *ApJ*, 709:1100–1118, Feb. 2010.

[3] O. Porth, C. Fendt, Z. Meliani, and B. Vaidya. Synchrotron radiation of collimating relativistic mhd jets. *ApJ*, submitted, 2011.

Ask me, I am around

Oliver Porth
Max-Planck-Institut für Astronomie
Konigstuhl 17
D-69117 Heidelberg
porth@mpia.de
Phone: (+49) 6221 528-315